Ranacyclins, a New Family of Short Cyclic Antimicrobial Peptides: Biological Function, Mode of Action, and Parameters Involved in Target Specificity[†,⊥,@]

M. Luisa Mangoni,[‡] Niv Papo,[§] Giuseppina Mignogna,[‡] David Andreu,[∥] Yechiel Shai,[§] Donatella Barra,*[,‡] and Maurizio Simmaco[‡]

Istituto Pasteur Fondazione Cenci Bolognetti, Dipartimento di Scienze Biochimiche, Ospedale S. Andrea, and CNR Istituto di Biologia e Patologia Molecolari, Università "La Sapienza", 00185 Roma, Italy, Department of Biological Chemistry, The Weizmann Institute of Science, Rehovot 76100, Israel, and Department of Experimental and Health Sciences, Universitat Pompeu Fabra, 08003 Barcelona, Spain

Received April 2, 2003; Revised Manuscript Received August 14, 2003

ABSTRACT: We report on two new cyclic 17-residue peptides that we named ranacyclins E and T, the first isolated from *Rana esculenta* frog skin secretions and the second discovered by screening a cDNA library from *Rana temporaria*. Ranacyclins have a loop region that is homologous with that of an 18-mer peptide, pLR, isolated from the skin of the Northern Leopard frog, *Rana pipiens*, with no reported antimicrobial activity. Here we show that ranacyclins and pLR have antimicrobial and antifungal activity. However, despite the high structural similarity, they differ in their spectrum of activity. The data reveal that ranacyclins and pLR have several properties that differentiate them from most known antimicrobial peptides. These include the following: (i) they adopt a significant portion of random coil structure in the membrane as revealed by ATR-FTIR and CD spectroscopy (50% for ranacyclin T and 70% for both ranacyclin E and pLR); (ii) they bind similarly to both zwitterionic and negatively charged membranes as revealed by using tryptophan fluorescence and surface plasmon resonance (SPR; BIAcore biosensor); (iii) they insert into the hydrophobic core of the membrane and presumably form transmembrane pores without damage to the bacterial wall, as revealed by SPR, ATR-FTIR, and transmission electron microscopy (TEM); and (iv) despite being highly and equally active in permeating bacterial spheroplasts and negatively charged membranes, they differ significantly in their potencies against target cells. Furthermore, a significant fraction of a given secondary structure is not prerequisite for membrane permeation and antimicrobial activity. However, increasing the fraction of a secondary structure and reducing peptide assembly in the membrane make it easier for the peptide to diffuse through the cell wall, which is different for each microorganism, into the cytoplasmic membrane.

The defense and offense systems of all organisms, including plants and humans, comprise peptide toxins, which are highly active on membranes. They serve as a nonspecific defense system that complements the highly specific cell-mediated immune response. The skin of frogs is one of the richest sources of such peptides that exhibit a broad spectrum of antimicrobial activity (*1*−*5*). These peptides have been shown to lyse a variety of microorganisms and cells including bacteria, fungi, and normal and cancer cells. A major group includes positively charged amphipathic peptides, most of which act predominantly on bacteria (*6*−*11*). Many studies aimed at elucidating their mode of action showed a correlation between their biological function and their ability to increase the permeability of model and target cell membranes (*12*−*19*). However, these studies only rarely addressed the issue of their different spectra of activities, because some are active predominantly on a variety of bacteria, others only on specific bacterial strains, and some on fungi and/or mammalian cells. Therefore, factors affecting target cell selectivity of antimicrobial peptides are not yet clear.

We have identified a putative peptide from a *Rana temporaria* skin cDNA library, and we have isolated a similar peptide from *Rana esculenta* skin secretion. These molecules, named ranacyclin T (for temporaria) and ranacyclin E (for esculenta), respectively, contain 17 amino acid residues with two cysteines forming a disulfide bridge. They differ from each other by only two amino acids at the N-terminal region. Ranacyclins share 13 amino acids in the loop region with pLR, an 18-mer peptide, isolated from the skin extract of the Northern Leopard frog *Rana pipiens* (*20*). pLR has been shown to have diverse biological functions which are not related to direct antimicrobial activity, such as activation of mast cells, induction of histamine release, and inhibition of granulocyte macrophage colony formation without the induc-

[†] This study was supported in part by grants from the Italian Ministero dell'Istruzione, Università e Ricerca (MIUR), Consiglio Nazionale delle Ricerche (Agenzia 2000), and Centro di Eccellenza BEMM (to D.B.) and by European Community Project QLK2-2000-00411 (to Y.S.).

[⊥] The nucleotide sequence of the mRNA coding ranacyclin T has been deposited in the GenBank/EMBL data band as entry AJ583866. The sequence of ranacyclin E will appear in the Swiss-Prot and TrEMBL database as entry P83663.

[@] This paper is dedicated to the memory of Professor Franco Tato.

* To whom correspondence should be addressed at the Dipartimento di Scienze Biochimiche, Università "La Sapienza", Piazzale Aldo Moro 5, 00185 Roma, Italy. Tel: +39 06 4456663. Fax: +39 06 4440062. E-mail: donatella.barra@uniroma1.it.

[‡] Università "La Sapienza".

[§] The Weizmann Institute of Science.

[∥] Universitat Pompeu Fabra.

10.1021/bi034521l CCC: $25.00 © 2003 American Chemical Society
Published on Web 11/04/2003

tion of neutrophil apoptosis. The sequences of ranacyclins and pLR are markedly different from most known lytic peptides isolated from the skin of frogs, which are mainly linear and adopt an amphipathic α-helix structure. More specifically, the 13 amino acid loop is a relatively rigid cyclic structure determined by the consensus polyproline motif Pro^{11}-Pro^{12}-Lys^{13}-Pro^{14} and the disulfide bridge between Cys^5 and Cys^{15}. Both ranacyclins T and E were synthesized and studied together with pLR for (i) their biological function on bacteria, fungi, and human erythrocytes; (ii) their ability to permeate the cytoplasmic membrane of bacteria by using fluorescence spectroscopy and β-galactosidase activity on the chromogenic ONPG substrate; (iii) their ability to bind and permeate zwitterionic and negatively charged vesicles by using surface plasmon resonance (SPR;[1] BIAcore biosensor) and fluorescence spectroscopy; and (iv) their structure and ability to penetrate into the hydrophobic core of the membranes and a membrane-mimetic environment by using circular dichroism (CD) and attenuated total reflectance Fourier transform infrared spectroscopy (ATR-FTIR). We found that ranacyclins and pLR have several properties that differentiate them from most known positively charged antimicrobial peptides: (i) they bind and insert similarly into the inner layer of both zwitterionic and negatively charged membranes, rather than lying onto the surface of the membrane; (ii) they adopt a secondary structure with a significant proportion of random coil structure; (iii) despite adopting predominantly unordered structure, they presumably form transmembrane pores rather than disintegrate the bacterial wall; and (iv) they significantly differ in their potencies against the different target cells despite being highly and equally active in permeating bacterial and negatively charged membranes. The results are discussed in the context of the role of ranacyclins and pLR as a part of the antimicrobial peptide pool in the skin of frogs, as well as their plausible mode of action, and the biophysical parameters that are responsible for the difference in their potencies and target specificity. Furthermore, the findings that peptides with significant random coil content preserve potent antimicrobial activity should assist in the future design of antimicrobial peptides as new target antibiotics, urgently needed because of the increasing resistance of pathogens to available drugs.

EXPERIMENTAL PROCEDURES

Materials. High-performance liquid chromatography-(HPLC-) grade solvents and sequence-grade chemicals were obtained from Carlo Erba Reagenti (Milan, Italy) and Applied Biosystems (Foster City, CA), respectively. Media for antimicrobial assays were purchased from Difco (BD Diagnostic Systems, Sparks, MD). Agarose (A 6013), isopropyl β-thiogalactopyranoside (IPTG), *o*-nitrophenyl β-D-galactopyranoside (ONPG), carbonyl cyanide *m*-chlorophenyl hydrazone (CCCP), 3-(4,5-dimethylthiazol-2-yl)-2,5-diphenyltetrazolium bromide (MTT), rifampicin, erythromycin, tetracycline, trypsin, proteinase K, egg phosphatidylcholine (PC), egg phosphatidylglycerol (PG), phosphatidylethanolamine (type V, from *Escherichia coli*; PE), cholesterol (Cho), *N*-octyl β-D-glucopyranoside (OG), and bovine serum albumin (BSA) were purchased from Sigma Chemical Co. (St. Louis, MO). 3,3′-Diethylthiodicarbocyanine iodide (diS-C_3-5) was obtained from Molecular Probes (Eugene, OR). All other reagents were of analytical grade. Buffers were prepared in double glass-distilled water.

Peptide Synthesis. Ranacyclins were synthesized as C-terminal carboxamides on *p*-methylbenzhydrylamine resin (0.45 mmol/g) at 0.1 mmol scale using Boc-based chemistry with in situ neutralization and dicyclohexylcarbodiimide-mediated coupling protocols in a 430A peptide synthesizer (Applied Biosystems). pLR peptide was prepared as a C-terminal carboxylic acid starting from 0.1 mmol of Boc-Arg(tosyl)-OCH_2-Pam-resin (0.7 mmol/g; Applied Biosystems) using standard protocols and finally cleaved from the resin with HF/anisole (9:1 v/v, 0 °C, 1 h). MALDI-TOF mass spectral analyses of the ranacyclin and pLR crude materials gave main peaks at *m*/*z* 1891.0, 1904.9, and 2137.2, respectively, in good agreement with the expected ($M + H^+$) structures. The crude peptides were dissolved to make 50 μM in 0.02 M Tris-HCl buffer, pH 8.0, and air-oxidized until conversion to the cyclic disulfide form was shown to be complete by HPLC (after 15−40 h). The resulting oxidation products were purified to near homogeneity (>98% by HPLC) by medium-pressure HPLC on a Nucleosil C_{18} column (2 × 30 cm) using 10−30% acetonitrile gradients in water with 0.05% trifluoroacetic acid (TFA). The purified cyclized peptides (10% overall yield) were confirmed by MALDI-TOF and amino acid analysis.

Molecular Cloning. A cDNA library from the skin of *R. temporaria*, prepared in pBlueScript as reported previously (*21*), was screened with a 150-bp fragment coding for the prepro region of the antimicrobial peptide brevinin-2E precursor (*22*). Positive clones were selected and analyzed by cleavage with restriction enzymes and nucleotide sequencing.

Collection and Purification of Frog Skin Secretion. Skin secretions from *R. esculenta* were obtained by mild electrical stimulation and collected by washing the animal with 0.05% acetic acid. Peptide HPLC fractionation was performed as previously reported (*22*).

Preparation of Small and Large Unilamellar Vesicles. SUVs were prepared by sonication of PE/PG (7:3 w/w) or PC/Cho (10:1 w/w) dispersions as previously described (*23*). LUVs were prepared by extrusion from the same lipids, as described in detail previously (*24*).

Antibacterial Activity of the Peptides. The antibacterial activity of the peptides was tested using an inhibition zone assay on agarose plates seeded with viable bacteria according to Hultmark et al. (*25*) (see, for details, the Appendix). The lowest concentration that inhibits the microbial growth in this type of assay was designated as the lethal concentration (LC). Seven different bacterial strains were used: the standard Gram-positive *Bacillus megaterium* Bm11 and the Gram-negative *E. coli* D21 and *E. coli* D22, the clinical isolate *Yersinia pseudotuberculosis* YP III, the human ocular pathogens *Staphylococcus lentus* and *Micrococcus luteus*, and the plant pathogen *Pseudomonas syringae* pv *tabaci*.

In Vitro Time-Killing Curves. The peptides were added to an exponential phase culture of *P. syringae* pv *tabaci* in phosphate-buffered saline (PBS; 35 mM phosphate buffer/

[1] Abbreviations: ATR-FTIR, attenuated total reflectance Fourier transform infrared; CD, circular dichroism; Cho, cholesterol; LUVs, large unilamellar vesicles; PC, egg phosphatidylcholine; PE, phosphatidylethanolamine; PG, egg phosphatidylglycerol; SPR, surface plasmon resonance; SUVs, small unilamellar vesicles.

0.15 M NaCl, pH 7.4, at 24 °C) containing about 10^5 cells/mL. Bacteria were then incubated at 30 °C, and 10 μL aliquots were withdrawn at different intervals and spread on agar plates. The number of surviving bacteria, expressed as the percentage of colony forming units (CFU), were counted after an overnight incubation at 30 °C.

Antifungal Activity. The anticandidal activity was assayed using the inhibition zone assay on Winge medium (WB)−agarose plates. Yeast cells were grown at 30 °C in 10 mL of WB (*26*) to an optical density value of 0.6 at 590 nm and diluted 300 times in 6 mL of WB−1% agarose. Three *Candida* species were used: the clinical isolate *Candida albicans* ATCC 10231, *Candida tropicalis*, isolated from human oral microbial flora, and *Candida guiller-mondii*, isolated from *R. esculenta* (*27*). The activity against the spores of the filamentous fungus *Phytophthora nicotianae* PG344, responsible for dangerous plant infections, was carried out in microplates. *P. nicotianae* was cultivated in potato dextrose agar (PDA) plates, and spore suspensions were prepared as follows: Fifteen-day-old colonies were scraped from the agar into sterile deionized water, and the suspension was filtered through Whatman 541 paper to obtain a zoospore eluate free of mycelial components (*28*). The spores were washed in sterile water and resuspended in WB medium at a final density of about 1×10^5 spores/mL. Subsequently, 75 μL of the spore suspension was placed in the wells of a microtiter plate, and 3 μL of a 2-fold dilution series of the peptides, dissolved in 20% ethanol, was added. The plates were then incubated at 30 °C, and the growth of the fungus was monitored macroscopically. The minimal inhibitory concentration (MIC) is defined as the lowest peptide concentration preventing visible growth after 20 h.

Hemolysis of Human Red Blood Cells. The hemolytic activity of the peptides was determined using fresh human erythrocytes. The blood was centrifuged, and the erythrocytes were washed three times with 0.9% NaCl. Peptide solutions were incubated with the erythrocyte suspension (1×10^7 cells/mL in 0.9% NaCl) at 37 °C for 2 h. Then, the extent of hemolysis was measured on the supernatant from the optical density at 415 nm. Hypotonically lysed erythrocytes were used as a standard for 100% hemolysis.

Effect of Membrane Potential on Antibacterial Activity. A culture of *E. coli* was pretreated with the uncoupler CCCP to collapse the transmembrane protonmotive force. Although oxidative phosphorylation is inhibited by CCCP, *E. coli* cells are able to grow in the presence of the protonophore when glucose is added as an energy source (*29*). Thus, a culture of *E. coli* D21 was grown overnight in a rich medium [50 mM 2-(*N*-morpholino)ethanesulfonic acid−Tris buffer, pH 7.5, 10 g/L tryptone, 5 g/L yeast extract, 5 mM K_2HPO_4, and 0.5% glucose] in the presence of 100 μM CCCP. Next, it was transferred to a fresh medium containing the uncoupler at the same concentration and grown to the logarithmic phase. The bactericidal activity of ranacyclin T was compared to that obtained using untreated cells. Bacteria were washed twice to remove the uncoupler and then diluted in PBS to 1×10^5cells/mL. The peptide, at a final concentration of 1 μM, was incubated at 30 °C. Aliquots, withdrawn after 30 and 60 min, were spread on LB plates for counting.

Permeation of the Cytoplasmic Membrane. The cytoplasmic membrane permeability in the presence of ranacyclins T and E was assayed by measuring the β-galactosidase activity on the chromogenic ONPG substrate as described in detail previously (*30*) (more details in the appendix). All of the results are the mean of three to five independent experiments.

Synergistic Effects with Conventional Antibiotics. Ranacyclins T and E were tested with rifampicin or erythromycin. Briefly, 4 nmol of each peptide was loaded into the wells punched in LB−1% agarose plates containing about 10^5 *Pseudomonas aeruginosa* ATCC 15692 cells and a sublethal concentration (5 μg/mL) of the antibiotics. After 12 h of incubation at 30 °C, the inhibition zone diameters were recorded.

CD Spectroscopy. CD spectra of the peptides were recorded with a Jasco J-500A spectropolarimeter after calibrating the instrument with (+)-10-camphorsulfonic acid. The spectra were scanned at 25 °C in a capped, quartz optical cell with a 0.5 mm path length. Spectra were obtained at wavelengths of 250−190 nm. Eight scans were taken for each peptide at a scan rate of 20 nm/min. The peptides were scanned at 1−50 μM in PBS and in the presence of 1% SDS. To quantify the different structures obtained, the CD spectra were processed using PEAKFIT software (Jandel Scientific, San Rafael, CA). The spectra accompanied by 13-data-point Savitsky−Golay smoothing were calculated to identify the positions of the component bands in the spectra. These wavelengths were used as initial parameters for curve fitting with Gaussian component peaks. The relative contents of the different secondary structure elements were estimated by dividing the areas of individual peaks, assigned to a specific secondary structure, by the whole area of the resulting bands (between 195 and 260 nm). The results of three independent experiments were averaged.

Localization of the Environment of Tryptophan. The fluorescence emission spectrum of tryptophan, at different peptide concentrations, was monitored in PBS and in the presence of vesicles composed of either PE/PG (7:3 w/w), a phospholipid composition typical of *E. coli* (*31*), or PC/Cho (10:1 w/w), a phospholipid composition used to mimic the outer leaflet of human erythrocytes (*32*), as previously described (*33*). Furthermore, proteinase K (10 μg/mL in PBS) was added to the peptides in PBS, and the resulting fluorescence was monitored. In these fluorometric studies, SUVs were used to minimize differential light scattering effects (*34*), and the lipid:peptide molar ratio was maintained high (>1000:1) so that the spectral contributions of free peptide would be negligible.

Binding Analysis by Surface Plasmon Resonance Biosensor. Biosensor experiments were carried out with a BIAcore 3000 analytical system (Biacore, Uppsala, Sweden) using an L1 sensor chip which forms lipid bilayers. We followed the protocol described previously (*35, 36*). Peptides at different concentrations were then injected onto the lipid surface until equilibrium has been reached and then washed out (see details in the Appendix). The maximal equilibrium response is designated as R_{eq} or RU_{max}. The equilibrium affinity constants were calculated from the relationship between the equilibrium binding response and the concentration of the peptide, *C*, using a steady-state affinity model (see details in the Appendix and also in ref *36*).

The sensorgrams for each peptide−lipid bilayer interaction were also analyzed by curve fitting using numerical integration analysis (*37*). We chose a curve-fitting algorithm that

FIGURE 1: Nucleotide sequence of the insert present in the clone Rt-26 and the corresponding amino acid sequence. The sequence of the mature peptide is underlined as well as the potential polyadenylation site. The vertical arrow indicates the probable site of cleavage by the signal peptidase.

describes a two-state reaction model (*35*) which, in terms of peptide−lipid interaction, corresponds to

$$P + L \underset{k_{d1}}{\overset{k_{a1}}{\rightleftharpoons}} PL \underset{k_{d2}}{\overset{k_{a2}}{\rightleftharpoons}} PL^*$$

where, in the first step, peptide (P) binds to lipids (L) to yield PL, which is changed to PL* in the second step. PL* cannot dissociate directly to P + L and may correspond to a partial insertion of the peptide into the lipid bilayer. Moreover, k_{a1}, k_{d1}, k_{a2}, and k_{d2} are the association and dissociation rate constants for the first and second steps, respectively, where k_{a1} has 1/(M s) units and k_{d1}, k_{a2}, and k_{d2} have 1/s units. Thus, the total affinity constant for the entire process, *K*, has 1/M units.

Increase in Membrane Permeability Induced by the Peptides. Membrane destabilization, which results in the collapse of the diffusion potential, was detected fluorometrically as previously described (*38*−*40*) (see details in the Appendix).

Transmembrane Potential Depolarization Assay with Bacterial Spheroplasts. The assay was done with the Gram-negative *E. coli* D21 spheroplasts, under the experimental conditions described previously (*41*). Bacterial spheroplasts [LPS and peptidoglycan-free bacteria (*42*)] were prepared by the osmotic shock procedure (*43*) (see details in the Appendix). The spheroplasts (used at the same concentration as in the biological activity assay) were incubated with 1 μM diS-C_3-5 until a stable reduction of fluorescence was achieved (around 60 min), indicating the incorporation of the dye into the bacterial membrane. Peptides at different concentrations were then added. Plasma membrane depolarization was monitored by observing the change in the intensity of the fluorescence emission of the membrane potential-sensitive dye diS-C_3-5 (excitation wavelength λ_{ex} = 620 nm, emission wavelength λ_{em} = 670 nm) after the addition of different concentrations of peptides.

ATR-FTIR Measurements. Spectra were obtained with a Bruker equinox 55 FTIR spectrometer equipped with a deuterated triglyceride sulfate (DTGS) detector and coupled to an ATR device as previously described (*33*). Briefly, a mixture of PE/PG (0.5 mg) alone or with peptide (~20 μg) was deposited on a ZnSe horizontal ATR prism. Infrared spectra were recorded, and the respective pure phospholipid spectra were subtracted to yield the spectra of only the peptide (see details in the Appendix). The relative contents of different secondary structure elements were estimated by dividing the areas of individual peaks, assigned to a specific secondary structure, by the whole area of the resulting amide I band. The results of four independent experiments were averaged.

Examination of Bacteria Morphology by Electron Microscopy. Samples containing *E. coli* D21 (1×10^6 CFU/mL) in LB medium were incubated with the peptides at their MIC and then centrifuged for 10 min at 300*g*. The pellets were resuspended, and a drop containing the bacteria was deposited onto a carbon-coated grid and negatively stained with 2% phosphotungstic acid (PTA), pH 6.8. The grids were examined using a JEOL JEM 100B electron microscope (Japan Electron Optics Laboratory Co., Tokyo, Japan).

RESULTS

Identification and Isolation of Ranacyclins. The clone Rt-26 was identified by screening a cDNA library from the skin of *R. temporaria* with a probe corresponding to the cDNA coding for the prepro region of the brevinin-2E precursor (*22*). The sequence of this clone is shown in Figure 1.

Table 1: Sequences, Retention Times, and Net Charge of the Peptides Investigated

Peptide	Sequence[a]	HPLC Retention Time[b] (min)	Net charge
Ranacyclin T	GAL**RGCWTKSYPPKPC**K-NH_2	25.41	+5
Ranacyclin E	SAP**RGCWTKSYPPKPC**K-NH_2	23.33	+5
pLR	LV**RGCWTKSYPPKPC**FVR	29.54	+4

[a] Conserved amino acids are boldfaced. Ranacyclins T and E are amidated at their C-termini. [b] A C_{18} reversed-phase analytical column was used. The peptides were eluted in 40 min using a linear gradient of 5−45% acetonitrile in water containing 0.05% TFA (v/v).

Excluding the poly(A) tail, this cDNA comprises 310 nucleotides, and its open reading frame can be translated into a 62 amino acid polypeptide with a typical feature of a peptide precursor. It starts with the signal peptide containing a cluster of hydrophobic residues, whereas the cleavage site for signal peptidase is most likely located after the cysteine in position 22 (*44*). After the acidic prosegment of 21 amino acids, the sequence corresponding to a 17-residue mature peptide is present in a single copy (Figure 1). This sequence is preceded by a Lys-Arg motif, which is a typical processing site for endoproteolytic cleavage, and is followed by the sequence Gly-Lys, as previously observed in the precursors of temporins (*21*). Thus, the predicted 17 amino acid end product, named ranacyclin T, containing a tryptophan residue in position 7 and two cysteine residues in positions 6 and 16, respectively, is likely to be amidated at its C-terminus. However, the mature product was not detected in *R. temporaria* skin secretion, possibly because of its scarce amount.

We synthesized ranacyclin T, and on the basis of its retention time and its absorbance at 280 nm, a similar peptide, differing by only two amino acids in the N-terminal region, was isolated from *R. esculenta* skin secretions and named ranacyclin E. Its retention time is 15.5 min, referring to the HPLC profile of skin secretion reported in Figure 6 of ref *22*. Ranacyclin E was found to contain a disulfide bridge. The sequences of the two *Rana* peptides and pLR (*20*) are shown in Table 1, together with their RP-HPLC retention times. They represent a novel family of loop-containing short antimicrobial peptides. Both ranacyclins share 13 amino acids of their central region with pLR, which is not amidated at the C-terminus (Table 1).

Biological Studies. (A) Antibacterial and Hemolytic Activities of the Peptides. The antibacterial activity of both ranacyclins and pLR was assayed against a representative set of microorganisms, including Gram-negative and Gram-positive species. Table 2 summarizes the results. Despite the very high sequence identity, their spectrum of antimicrobial activity differs considerably. Whereas ranacyclins were active against most of the tested bacteria, with ranacyclin T being the most potent one, pLR was active only against a few sensitive strains of Gram-positive bacteria.

The peptides were also tested for their hemolytic activity against human erythrocytes. Table 2 shows that pLR and ranacyclin E have the highest hemolytic activity. Note that whereas the hemolytic activity of ranacyclin E was detected already after 30 min, pLR showed hemolytic activity only after 1 h incubation with the erythrocytes.

Table 2: Antimicrobial and Hemolytic Activities of the Peptides[a]

microorganisms	ranacyclin T	ranacyclin E	pLR
Gram-negative bacteria			
E. coli D21[b]	30	NA[e]	NA
E. coli D22[b]	NA	NA	NA
Y. pseudotuberculosis YP III	5	9	NA
Ps. syringae pv *tabaci*	16	80	NA
Gram-positive bacteria			
B. megaterium Bm11[b]	3	3	20
S. lentus	10	7	50
M. luteus	8	5	10
fungi cells			
C. albicans[c] ATCC 10231	22	NA	NA
C. tropicalis[c]	14	7.4	11
C. guiller-mondii[c]	1.0	3.4	6.6
P. nicotianae spores[d]	16	32	75
% hemolysis at 100 μM[f]	20	55	85

[a] The antibacterial activity was determined with the inhibition zone assay on agarose plates and is expressed as LC (μM). Results are the mean of three independent experiments, each performed in duplicate, with standard deviation not exceeding 20%. [b] Streptomycin-resistant strains (up to 100 μg/mL). [c] The antifungal activity was determined by the inhibition zone assay in WB−1% agarose. [d] The antifungal activity was determined in WB liquid medium and is expressed as MIC (μM). [e] NA, not active (LC above 100 μM). [f] Hemolytic activity after 2 h.

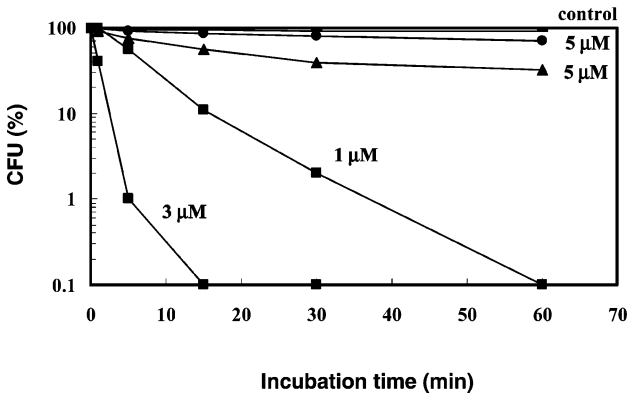

FIGURE 2: In vitro time-killing curve of ranacyclin T (■), at two concentrations, ranacyclin E (▲), and pLR (●) against *Ps. syringae* pv *tabaci*.

(B) Kinetics of Bacterial Killing (Time-Killing Curve). A high potency against *Ps. syringae* pv *tabaci* was displayed by ranacyclin T at a peptide concentration range of 1−3 μM. A time-killing dependence on peptide concentration was observed, and at 3 μM, the peptide killed about 10^5 cells/mL in 15 min (Figure 2). In contrast, ranacyclin E had much lower activity even at the highest peptide concentration used (5 μM). As expected, no killing activity was detected for pLR (at 5 μM). Similar patterns were also observed with several other bacterial strains (data not shown). The fast kinetics indicate the membrane as the target of ranacyclin T, although it cannot explain why the two others are not active.

(C) Antifungal Activity of the Peptides. Antifungal activity was assayed against representative pathogenic fungi (Table 2). Amphotericin B served as a control. The trend in antifungal activity was similar to that found in the antimicrobial activity. Overall, ranacyclin T was the most active peptide

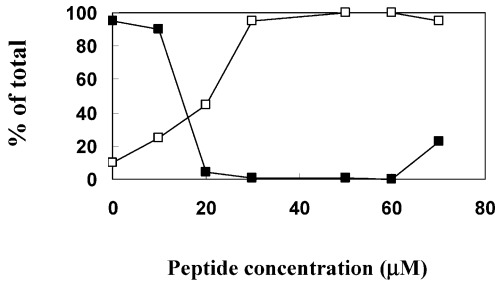

FIGURE 3: β-Galactosidase activity in the culture filtrate of *E. coli* D21 (empty symbols) and cell viability (filled symbols), expressed as percent of the total, after treatment with ranacyclin T at different concentrations. The enzyme activity is measured on the culture filtrate following the hydrolysis of ONPG at 420 nm. The enzyme activity detected in the control (bacteria without peptide) was subtracted from all values.

against all of the strains tested, ranacyclin E to a lesser extent, and pLR was the least active peptide. Importantly, amphotericin B was not active on *C. guiller-mondii*. Furthermore, whereas the two ranacyclins were also active on *P. nicotianae* spores and hyphae, both pLR and amphotericin B were practically inactive (data not shown).

Mode of Action Studies with Bacteria. (A) Effect of Membrane Potential on Antibacterial Activity. It has been shown previously that peptides that form "pores" or "channels" are inserted into the membrane in a voltage-dependent manner. With bacteria, their insertion is facilitated by a transmembrane potential of ~140 mV. Such peptides should have a reduced bactericidal effect on bacteria pretreated with an uncoupler that discharges the pH gradient and destroys the membrane potential. To investigate this possibility, we used the most active peptide ranacyclin T. *E. coli* D21 cells were preincubated with CCCP and then with ranacyclin T. The data reveal a similar percentage of CFU detected 30 min (2−3%) and 60 min (0%) after adding peptide with and without CCCP treatment.

(B) Permeation of the Cytoplasmic Membrane. Further support for the bacterial membrane as the target of ranacyclins is the loss of cytoplasmic membrane integrity after peptide treatment. This was detected by measuring the cytoplasmic β-galactosidase activity in the filtrate of the *E. coli* D21 culture after incubation with the peptides. The results demonstrate a progressive enzyme release at increasing concentrations of ranacyclin T (Figure 3) and ~100% enzyme activity even at the lowest ranacyclin T concentration (30 μM), shown to cause total bacterial death. In contrast to ranacyclin T, a 10-fold higher concentration of ranacyclin E was necessary to kill the same amount of *E. coli* D21 cells, but no β-galactosidase activity was detected in the supernatant. Nevertheless, ranacyclin E was able to permeate the bacterial cytoplasmic membrane to substrates of small molecular size such as ONPG, because high enzymatic activity was detected in the whole bacterial culture after peptide treatment.

(C) Synergistic Effect between Ranacyclins and Conventional Antibiotics. Ranacyclins were found to display a synergistic effect in combination with classical antibiotics against *Ps. aeruginosa* ATCC 15692, which has a highly impermeable outer membrane (*45*). We used LB−agarose plates containing the bacteria and a sublethal concentration of rifampicin or erythromycin (5 μg/mL). Consequently, a growth inhibition zone was formed around the wells containing 4 nmol of ranacyclin T, an amount that is not active alone. The same amount of ranacyclin E inhibited bacterial growth in the presence of rifampicin, but not of erythromycin. No synergistic effect was observed when pLR was used. These results further support the notion that ranacyclins act on the bacterial membrane.

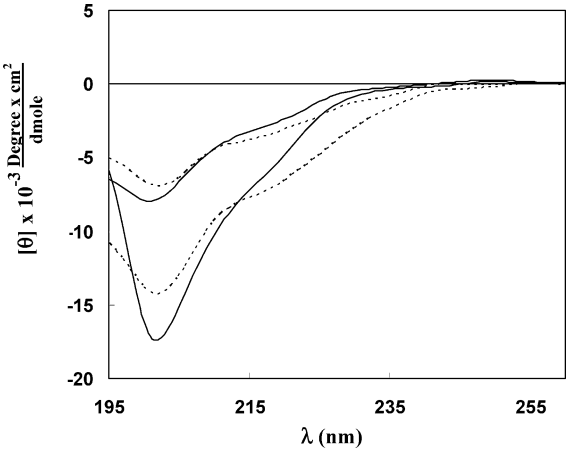

FIGURE 4: CD spectra of ranacyclin T, ranacyclin E, and pLR peptides. Spectra were taken at 50 μM peptide dissolved in PBS (solid line) and 1% SDS (dashed line). The upper lines are for ranacyclin T, and the two lower lines are for ranacyclin E. The pLR spectra overlap that of ranacyclin T in PBS and that of ranacyclin E in SDS and therefore are not shown.

Mode of Action Studies with Model Membranes. (A) Secondary Structure and Aggregation of the Peptides in PBS and SDS Solutions Determined by Circular Dichroism Spectroscopy. The secondary structure of the peptides was determined in PBS and 1% SDS solutions (mimicking a membrane environment) at a concentration range of 1−50 μM (the spectra at 50 μM are shown in Figure 4). We found that the peptides have a partial β-sheet structure in PBS (20% for ranacyclin T and pLR, 15% for ranacyclin E, and the rest random coil), but their spectra are concentration-independent. This suggests that either the peptides exist, at least partially, as oligomers or, alternatively, the β-sheet structure is due to an intramolecular arrangement because of ring structure (see also the following paragraph). In 1% SDS, both pLR and ranacyclin E are more unordered (70% random coil) than ranacyclin T (50% random coil) (Figure 4), in agreement with the FTIR studies.

(B) Detection of the Aggregation State of the Peptides in Solution. The emission maxima of the peptides were measured in PBS before and after enzymatic degradation (peptide degradation was confirmed by RP-HPLC). We found that all of the peptides displayed a red shift (4−8 nm) after enzymatic degradation, due to the relocation of the tryptophan to a less hydrophobic environment (spectra not shown). This suggests that the peptides are at least partially aggregated in solution, in agreement with the CD spectroscopy data.

(C) Interaction of the Peptides with Phospholipid Membranes. The fluorescence emission spectrum of the tryptophan was monitored in the presence of vesicles composed of PE/PG (7:3 w/w) or PC/Cho (10:1 w/w). The data reveal that there is no significant difference between the environments of tryptophan in PC/Cho compared with PE/PG (1−3 nm). Furthermore, in both lipids the environment is only mildly hydrophobic (344−349 nm). In addition, whereas the

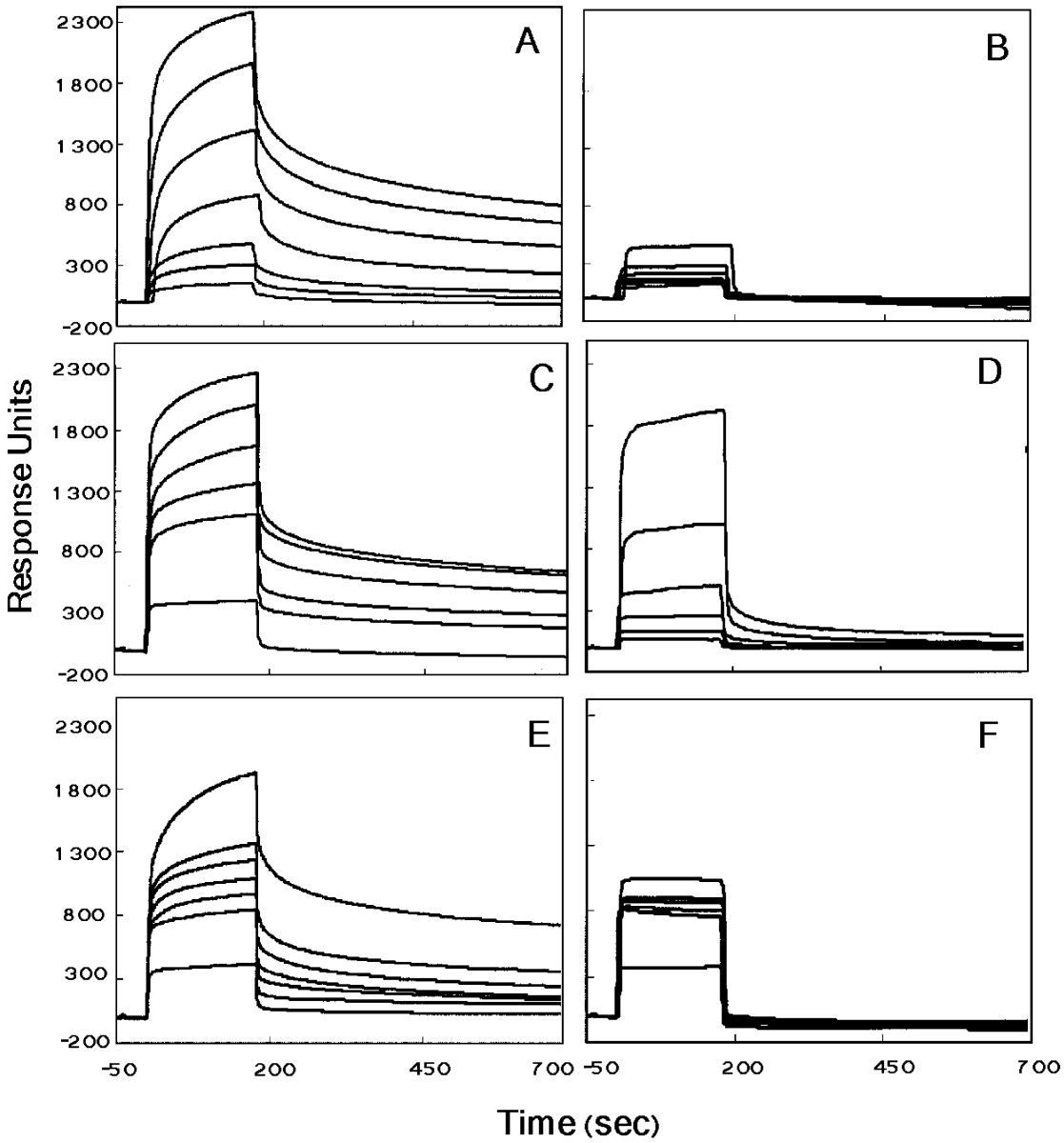

FIGURE 5: Sensorgrams of the binding between various concentrations of ranacyclin T (panels A, B), ranacyclin E (panels C, D), and pLR (panels E, F) and the lipid bilayer (L1 chip): PE/PG (7:3 w/w) (panels A, C, and E) and PC/Cho (10:1 w/w) (panels B, D, and F). All of the peptides are at concentrations of 1.56, 3.125, 6.25, 12.5, 25, 50, and 100 μM. Note that, in each panel, the curves with higher intensity correspond to the higher peptide concentration.

fluorescence intensity of ranacyclins was high, the fluorescence intensity of pLR was markedly reduced. This quenching can be due to a further oligomerization of the peptide in the membrane (supported by ATR-FTIR studies).

(D) Binding Affinity of the Peptides to Lipid Bilayers Measured by Surface Plasmon Resonance. (i) A Steady-State Affinity Model for Peptide Binding to Membranes. PE/PG (7:3 w/w) and PC/Cho (10:1 w/w) bilayers were absorbed onto an L1 bilayer sensor chip. Typical sensorgrams of the binding between ranacyclin T, ranacyclin E, and pLR with bilayers are shown in Figure 5. The sensorgrams of the binding between all of the peptides with PE/PG showed similar response levels (Figure 5, panels A, C, and E). However, the sensorgrams of the binding between ranacyclin T with PC/Cho showed significantly lower response levels compared with ranacyclin E and pLR (Figure 5, panels B, D, and F). Note that the concentrations of the peptides in the entire assay were similar. The sensorgrams revealed that the RU signal intensity increases as a function of the peptide concentration. This indicates that the amount of peptide bound to the lipids is proportional to the increase in peptide concentration.

(ii) A Two-State Model for the Peptide Binding to Membranes. We employed numerical integration analysis that uses nonlinear analysis to fit an integrated rate equation directly to the sensorgrams (*35*). When fitting the peptide sensorgrams globally (using different concentrations of the peptides) with the simplest 1:1 Langmuir binding model, a poor fit was obtained (data not shown), confirming that this model does not represent the lipid binding mechanism of the peptides investigated. However, a significantly improved fit was obtained using numerical integration of the two-state reaction model of the binding sensorgrams. This model reflects a two-step process in the interaction of the peptides with lipid bilayers: the first step is the actual binding, and the second is the insertion of the peptide into the membrane. A set of peptide sensorgrams with seven different peptide concentrations was used to estimate the kinetic parameters.

Table 3: Association (k_{a1}, k_{a2}) and Dissociation (k_{d1}, k_{d2}) Rate Constants in Bilayers Determined by Numerical Integration Using the Two-State Reaction Model[a]

peptides	lipid	k_{a1} [1/(M s)]	k_{d1} (1/s)	K_1 ($\times 10^4$ 1/M)	k_{a2} (1/s)	k_{d2} (1/s)	K_2	K ($\times 10^5$ 1/M)
ranacyclin T	PC/Cho	10.2 (±0.7)	0.00061 (±0.00009)	1.6	0.41 (±0.05)	0.029 (±0.001)	14.0	2.2 (±0.01)
	PE/PG	13.0 (±0.8)	0.00050 (±0.00009)	2.0	0.60 (±0.06)	0.025 (±0.004)	24.0	4.8 (±0.8)
ranacyclin E	PC/Cho	13.5 (±0.7)	0.00065 (±0.00006)	2.0	0.47 (±0.05)	0.023 (±0.002)	20.0	4.0 (±0.7)
	PE/PG	13.9 (±1.1)	0.00055 (±0.00007)	2.5	0.50 (±0.04)	0.024 (±0.002)	21.0	5.2 (±0.9)
pLR	PC/Cho	12.1 (±0.9)	0.00047 (±0.00009)	2.6	0.39 (±0.07)	0.027 (±0.003)	20.0	5.2 (±0.6)
	PE/PG	15.3 (±1.2)	0.00052 (±0.00007)	2.9	0.42 (±0.01)	0.025 (±0.001)	16.8	4.9 (±0.7)

[a] The affinity constants K_1 and K_2 are for the first ($K_1 = k_{a1}/k_{d1}$) and second ($K_2 = k_{a2}/k_{d2}$) steps, respectively, and the affinity constant (K), determined as (k_{a1}/k_{d1})(k_{a2}/k_{d2}), is for the complete binding process.

The average values for the rate constants obtained from the two-state model analysis are listed in Table 3 along with the affinity constant values, *K*. The data reveal about a 2-fold higher affinity of ranacyclin T to PE/PG compared with PC/Cho, whereas ranacyclin E and pLR have similar affinities to both types of lipids. These data partially explain the lower hemolytic activity of ranacyclin T compared with that of the other two peptides. Note that all of the peptides have similar affinities toward PE/PG bilayers, despite the fact that both ranacyclins contain one additional positive charge compared with pLR. This suggests that the higher hydrophobicity of pLR compensates for the lack of one positive charge. Furthermore, regarding the steps involved in the binding process, the data reveal that (i) the higher affinity of ranacyclin T to PE/PG compared with PC/Cho membranes is predominantly due to the second step and (ii) the value of the equilibrium constant of the second step for all of the peptides resembles that of peptides that insert into the hydrophobic core of the membrane, rather than lying on the outer surface (*36*). The experiments were repeated three times with a standard deviation of 10%. Previous studies confirmed that binding constants derived by using SPR are similar to those obtained by other methods (*35*, *36*, *46*−*49*).

(E) Secondary Structure of the Peptides in the PE/PG Phospholipid Membrane As Determined by FTIR Spectroscopy. The amide I region spectra of ranacyclin T, ranacyclin E, and pLR bound to PE/PG (7:3 w/w) multibilayers (after deuterium exchange) were examined. Secondary derivatives, accompanied by 13-data-point Savitsky−Golay smoothing, were calculated to identify the positions of the component bands in the spectra (figure not shown). These wavenumbers were used as initial parameters for curve fitting with Gaussian component peaks. Assignment of the different secondary structures to the various amide I regions was calculated according to the values taken from refs *50*−*53* and our previous results (*54*−*56*). The relative areas assigned to the corresponding structures of the peptides in PE/PG (7:3 w/w) are summarized in Table 4.

The data reveal a significant similarity between the structures of ranacyclin E and pLR when bound to membranes. Both peptides have a predominantly random coil structure in the membrane, in agreement with the CD spectroscopy results (Figure 4). In contrast, ranacyclin T is significantly more structured and adopts 50% β-sheets, aggregated strands, and turns (Table 4). The higher fraction of aggregated strands found in ranacyclin T and pLR could result from aggregation due to intermolecular hydrophobic interactions within these peptides, which are more hydrophobic than ranacyclin E. Note that most of the β-sheet structure found in pLR is in an aggregated form. Similar results were obtained when 1:120 or 1:60 peptide:lipid molar ratios were used.

Table 4: Peptide Structure As Determined by ATR-FTIR Spectroscopy from the Deconvolution of the Amide I Bands of the Peptides Incorporated into the PE/PG Multibilayers[a]

peptide	aggregated strands (%)	β-sheet (%)	random coil (%)	β-turn (%)
ranacyclin T	20 ± 3	17 ± 2	50 ± 3	12 ± 1
ranacyclin E	10 ± 2	15 ± 1	70 ± 3	5 ± 1
pLR	19 ± 2		70 ± 2	11 ± 1

[a] A 120:1 lipid:peptide molar ratio was used. The results are the average of four independent experiments.

(F) Orientation of the Phospholipid Membrane and Effect of the Peptides on the Phospholipid Acyl Chain Order. Polarized ATR-FTIR spectroscopy was used to determine the orientation of the lipid membrane with or without a bound peptide. The symmetric [$\upsilon_{sym}(CH_2) \approx 2853$ cm^{-1}] and the antisymmetric [$\upsilon_{sym}(CH_2) \approx 2922$ cm^{-1}] vibrations of lipid methylene C−H bonds are perpendicular to the molecular axis of a fully extended hydrocarbon chain. Thus, measurements of the dichroism of infrared light absorbance can reveal the order and orientation of the membrane sample relative to the prism surface. The effect of the peptides on the acyl chain order was estimated by comparing the CH_2 stretching dichroic ratio of PE:PG phospholipid multibilayers alone with that obtained with membrane-bound peptide. The calculated values based on the antisymmetric vibrations were found to be 1.28, 1.39, 1.44, and 1.60 for free lipids, ranacyclin T, ranacyclin E, and pLR incorporated in the lipid, respectively. Similar results were obtained on the basis of the symmetric vibrations. The data reveal that the incorporation of all the peptides has a significant effect on the acyl chain order of the lipid membranes, compared with what has been found with most antimicrobial peptides. Interestingly, the order of the effect correlates with the hydrophobicity of the peptides, as revealed by RP-HPLC (Table 1).

(G) Increase in Membrane Permeability Induced by the Peptides. Dissipation of diffusion potential experiments was used to test whether the peptides can increase the permeability of LUVs. The peptides were mixed at various concentrations with vesicles pretreated with the fluorescent dye, diS-C_3-5, and valinomycin, and the maximum recovery levels, reached as a function of the lipid:peptide molar ratio, were determined (Figure 6). The data reveal that all of the peptides have similar activity in increasing the permeability of PE/PG membranes despite major differences in their antibacterial activities (Figure 6, panel B). Furthermore, there

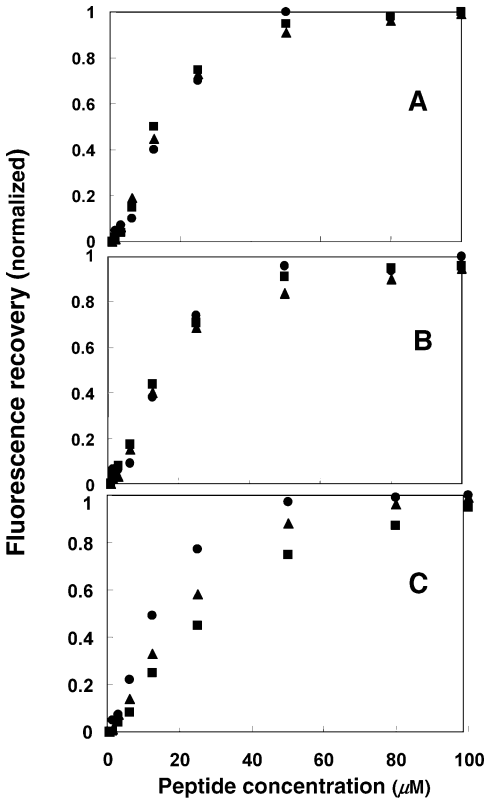

FIGURE 6: Maximal dissipation of the diffusion potential in the membrane of *E. coli* D21 spheroplasts (panel A), PE/PG (7:3 w/w) LUVs (panel B), and PC/Cho (10:1 w/w) LUVs (panel C) induced by ranacyclin T (■), ranacyclin E (▲), and pLR (●). The peptides were added to spheroplasts, PE/PG LUVs, or PC/Cho LUVs that were preequilibrated with the fluorescent dye diS-C_3-5 for 60 min. Fluorescence recovery was measured 1−120 min (at 5 min intervals) after the peptides were added, and its maxima were reported.

is a difference, albeit slight, between the abilities of the peptides to increase the permeability of the PC/Cho membranes (Figure 6, panel C). The order of activity correlates with the order of the hemolytic activity.

(H) Depolarization of the Membrane Potential of Bacterial Spheroplasts. To test whether factors other than the ability to interact with the bacterial plasma membrane are important for antibacterial activity, we performed transmembrane potential depolarizing experiments with both bacteria and bacterial spheroplasts (LPS and peptidoglycan-free bacteria). In the case of the spheroplasts, we used the Gram-negative *E. coli* D21 spheroplasts. The conditions were similar to what has been reported previously (*41*). The bacterial concentrations were similar to those used in the antibacterial assay. Panel A of Figure 6 shows the dose-dependent dissipation of the transmembrane potential of the spheroplasts. The data reveal that, despite the differences in the LC values for *E. coli* D21, all of the peptides possess similar activities in the dissipation of the transmembrane potential of this bacterial strain. These data correlate with similar activities of the peptides in increasing the permeability of PE/PG membranes (Figure 6, panel B).

(I) Electron Microscopy Visualization of Bacterial Lysis. The effect of the three peptides on the morphology of *E. coli* was visualized using transmission electron microscopy. Experiments were done at concentrations corresponding to their MIC values and revealed no differences in the morphology of the treated bacteria compared to the untreated ones (figure not shown).

DISCUSSION

Here we report on the identification and mode of action of ranacyclins, two new short and cyclic antimicrobial and antifungal peptides derived from the skin of frogs. They were studied along with a newly reported and highly homologous peptide, pLR, which was identified as a histamine-releasing peptide, with no hemolytic activity (*20*). We observed that pLR has both antimicrobial and antifungal activities, although with a narrower spectrum of action compared with the ranacyclins. Moreover, it displays the highest hemolytic activity among the three peptides, but only if incubated with erythrocytes more than 30 min, the time reported by Salmon et al. (*20*), in which no hemolytic activity was observed. The present study suggests that pLR and ranacyclins are indeed part of the frog's defense mechanism against microorganisms. In addition, ranacyclins and pLR are good models to study parameters that are involved in efficient biological activity and target specificity. This is because they share ~70% identity, but they significantly differ in their spectra of activity. This raises the question whether they all act via a similar mechanism. Since one of the targets of most antimicrobial peptides is the bacterial membrane, we performed studies along this line using both intact cells and liposomes. In addition, studies were conducted to determine the biophysical differences between the three peptides that might be responsible for their different activities. That the membrane is at least part of the target of the three peptides investigated is based on the following findings: (i) they strongly bind and increase the permeability of phospholipid membranes; (ii) their antimicrobial activity does not depend on the bacterial membrane potential; (iii) there is a synergistic effect between the peptides and antibiotics against antibiotic-resistant bacterial strains; (iv) the kinetics of bacteria killing is fast; and (v) the peptides depolarize the transmembrane potential of bacterial spheroplasts and increase the permeability of intact bacteria.

Biophysical Properties of the Peptides. Antimicrobial peptides, in general, vary significantly in their sequences, suggesting that a specific sequence is not crucial for biological activity. Here, only small changes in amino acid composition in the N- and C-terminal tails of ranacyclins and pLR resulted in a significant difference in their biological potencies. We found that these differences in activity could be due to differences in several intrinsic biophysical properties that are important for traversing of the microorganism's wall into the cytoplasmic membrane, rather than differences in their ability to permeate this membrane. The following characteristics were shown to differ among the three peptides: the peptide hydrophobicity, the oligomeric state in solution and membranes, the net positive charge, and the peptide structure.

pLR contains the most hydrophobic N- and C-terminal regions (Table 1), which make the peptide more hydrophobic than the two ranacyclins as revealed by its higher RP-HPLC retention time (Table 1). This hydrophobicity might contribute to its ability to oligomerize better in membranes (supported by FTIR studies) and solution (supported by CD spectroscopy and tryptophan blue shift). Earlier studies

showed that peptides that oligomerize in solution, and as a result increase their size, do not traverse efficiently through the outer surface into the inner membrane of Gram-negative bacteria (*33*, *43*, *57*). Therefore, the higher oligomeric state of pLR could explain its inactivity toward Gram-negative bacteria (Table 2), although it is able to permeate the inner membrane of *E. coli* similarly to the ranacyclins (Figure 6). Tryptophan blue shift experiments also suggest that ranacyclin T and, to a lesser extent, ranacyclin E are oligomers in solution. This might explain why ranacyclin E is more active than pLR but cannot explain why ranacyclin T has the highest activity compared with both pLR and ranacyclin E (this latter point will be discussed along with the structure of the peptides and their oligomeric state in the membrane, determined by using FTIR spectroscopy). Furthermore, whereas ranacyclins are amidated at their C-termini, thus having a net +5 charge, pLR has a free C-terminal carboxylate, which results in a net charge of +4: both changes are known to reduce antimicrobial activity (*58*).

The ability of the peptides to permeate intact Gram-negative bacteria (that contain both inner and outer membranes; Figure 3) correlated with their LC values (Table 2). In contrast, BIAcore studies revealed that all of the peptides bind similarly to PE/PG model membranes that mimic bacterial membranes and that most of the binding energy is the result of the first step, i.e., the binding to the outer surface (Figure 5 and Table 3). Furthermore, potential depolarization experiments with PE/PG and PC/Cho membranes and bacterial spheroplasts (containing only the inner membrane) revealed similar activity for all three peptides (Figure 6). This further supports our assumption that the difference between the antimicrobial activities of the peptides is not the result of differences in their ability to bind and permeate the bacterial membranes but rather to diffuse and reach them, probably via a process described as self-promoted uptake (*59*).

Structural Aspects in the Peptide Activity. The loop regions of pLR and ranacyclins, which compose most of the peptides, are identical. Therefore, we could predict that they adopt a similar structure and organization. However, there are some significant differences as revealed by FTIR and CD spectroscopy (Figure 4, Table 4).

The overall structures of ranacyclin E and pLR are similar when bound to negatively charged PE/PG membranes. Both peptides have predominantly random coil structures (70%), in contrast to ranacyclin T which is more structured (50% random coil). This might explain in part the higher activity of ranacyclin T compared with the two others. Furthermore, the entire β-sheet fraction of pLR is present only in oligomeric form, whereas ranacyclin E and T have a similar fraction of β-sheet component which is not aggregated (15−17%, Table 4). The increasing fraction of a secondary structure can explain further why ranacyclin T is the most potent peptide and pLR is the least potent one, mostly against Gram-negative bacteria.

Ranacyclins and pLR possess hemolytic activity in addition to their antimicrobial activity. Ranacyclin T is the least active whereas ranacyclin E and pLR are the most active. This can be explained at least partially by the lower affinity of ranacyclin T to PC/Cho, which mimics eukaryotic cell membrane (Figure 5). However, this difference can be more significant in erythrocytes, since the peptides bind first to the negatively charged glycocalix layer and then diffuse into the cytoplasmic membrane. The lower net positive charge of pLR compared with that of ranacyclins makes it easier for pLR to partition from the glycocalix layer into the PC membrane.

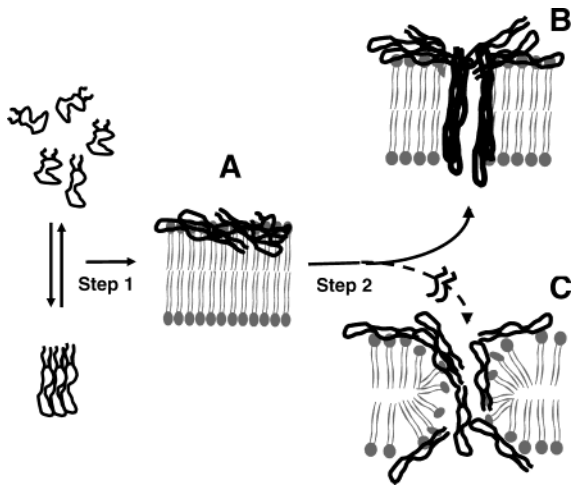

FIGURE 7: Schematic representation of a possible mechanism of pore formation by ranacyclins and pLR. Peptides bind in the first step predominantly by hydrophobic interactions and align parallel to the outer membrane surface (A). Increasing peptide concentration results in the insertion of the peptides into the hydrophobic core of the membrane to form transmembrane pores (B). These pores are different from the transient pores formed by most antimicrobial peptides that interact solely with the lipid headgroup (C).

Interestingly, since fungi mimic eukaryotic cells, we would expect a trend in antifungal activity similar to that of hemolytic activity. In contrast, the order of activity against the set of fungi tested is similar to that found in the antibacterial activity. A plausible explanation is that fungi do not contain the glycocalix layer and have thick walls compared to the red cells. Since all of the peptides bind strongly and permeate zwitterionic membranes, the differences in their activities should reside in the differences in their ability to diffuse into the cytoplasmic membrane of fungi, which is the same trend found in the antibacterial activity.

Mode of Action of Ranacyclins and pLR. An interesting finding in this study is that the peptides, despite being short, cyclic, and lacking of an amphipathic secondary structure, can insert into the hydrophobic core of the membrane and presumably form pores. This conclusion is based on several observations. (i) The peptides increase the permeability of the cytoplasmic membrane of bacteria and model phospholipid membranes, as shown respectively in Figures 3 and 6, but without disrupting the integrity of the bacteria as revealed by TEM (figure not shown). (ii) The peptides insert into the hydrophobic core of the membrane and disrupt the acyl chain order similarly to pore-forming peptides, such as melittin (*56*) and the α5 helix of δ-endotoxin (*60*), as revealed by the ATR-FTIR studies (see relevant Results section) (*13*). (iii) The peptides bind similarly to zwitterionic and negatively charged membranes, indicating a major contribution of the hydrophobic core of the membrane to the binding process, compared with electrostatic interaction between most antimicrobial peptides and the lipid headgroups. (iv) The binding of the peptides to both PC/Cho and PE/PG membranes

determined by using BIAcore biosensor could be fitted to a two-step model: binding to the outer leaflet followed by insertion into the bilayer. We found that the rate constants of the second step are similar to those obtained with pore-forming peptides such as melittin (*36*). It should be noted, however, that these pores are formed only after a threshold concentration of bound peptide has been reached, similarly to what has been described in the "carpet" mechanism (*61*). This assumption is based on the high concentration of peptides required to permeate spheroplasts and model membranes, compared with that required when a pore-forming peptide is used, such as pardaxin (*40*, *62*). However, once a threshold concentration has been reached, they insert into the hydrophobic core of the membrane and form pores, in contrast to most antimicrobial peptides that are in contact with the lipid headgroup through all of the permeation process (see Figure 7). Formation of aggregated channels/pores by nonamphipathic α-helices was proposed also by Hancock and co-workers (*41*).

APPENDIX

Antibacterial Activity of the Peptides. The antibacterial activity of the peptides was tested according to Hultmark et al. (*25*). Bacteria were grown in Luria−Bertani broth (LB) to an OD_{590nm} of 1. Bacteria in mid-logarithmic phase were diluted in LB medium, and about 2×10^5 colony forming units (CFU) was added to 6 mL of LB−1% agarose poured into Petri dishes. A 1 mm layer gel was formed, and 3 mm diameter wells were punched, to which 3 μL aliquots of the serially diluted peptide solutions, prepared in 20% ethanol, were introduced. After an overnight incubation at 30 °C, the inhibition zone diameters were measured and the lethal concentration (LC) was calculated.

Permeation of the Cytoplasmic Membrane. E. coli D21 was grown to logarithmic phase in LB broth in the presence of 1 mM IPTG to induce the enzyme. The cells were centrifuged and diluted to an OD_{590} of 0.35 in 10 mM sodium phosphate buffer, pH 7.4. About 3×10^6 cells were incubated with the peptides at different concentrations for 60 min at 30 °C. The bacterial culture was filtered with a 0.2 μm filter, 2 mM ONPG was added to the filtrate, and its hydrolysis was followed spectrophotometrically at 420 nm. The total enzyme activity was measured after the same number of cells were treated, in the absence of peptides, with 0.1% SDS/chloroform. For ranacyclin E, the enzyme activity was measured also in the whole bacterial culture after peptide treatment. All of the results are the mean of three to five independent experiments.

Binding Analysis by Surface Plasmon Resonance Biosensor. Biosensor experiments were carried out with a BIAcore 3000 analytical system (Biacore, Uppsala, Sweden) using an L1 sensor chip (BIAcore) that contains hydrophobic aliphatic chains with exposed polar headgroups. Thus, when in contact with vesicles, a lipid bilayer is formed. We followed the protocol described by Mozsolits et al. (*35*). Briefly, PBS (pH 6.8) was used as the running buffer, whereas the washing solution was 40 mM OG, and the regenerating solution was 10 mM NaOH. All solutions were freshly prepared, degassed, and filtered through 0.22 μm pores. Experiments were done at 25 °C. After the BIAcore 3000 instrument was cleaned according to the manufacturer's instructions, it was left running overnight using Milli-Q water as eluent to thoroughly wash all liquid handling parts of the instrument. The L1 chip was then installed and the alkanethiol surface was cleaned by an injection of 40 mM nonionic detergent OG (25 μL), at a flow rate of 5 μL/min. PE/PG (7:3 w/w) and PC/Cho (10:1 w/w) SUVs (80 μL, 0.5 mM) were then applied to the chip surface at a low flow rate (2 μL/min). To remove any multilamellar structures from the lipid surface, NaOH (50 μL, 10 mM) was injected at a flow rate of 50 μL/min, which resulted in a stable baseline corresponding to the lipid bilayer linked to the chip surface. The negative control BSA was injected (25 μL, 0.1 mg/μL in PBS) to confirm complete coverage of the nonspecific binding sites. The bilayer linked to the chip surface was then used as a model cell membrane surface to study the peptide−membrane binding.

Peptide solutions (a 15 μL PBS solution of 1.56−100 μM peptide) were injected on the lipid surface at a flow rate of 5 μL/min. PBS alone was then replaced by the peptide solution for 15 min to allow peptide dissociation. Surface plasmon resonance (SPR) detects changes in the reflective index of the surface layer of peptides and lipids in contact with the sensor chip. A sensorgram was obtained by plotting the SPR angle against time. The peptide−lipid binding event was analyzed from a series of sensorgrams collected at seven different peptide concentrations.

The system reached binding equilibrium during injection of the sample, and therefore the affinity constant could be calculated from the relationship between the equilibrium binding response (R_{eq} or RU_{max}) and the peptide concentration, C, using a steady-state affinity model. The affinity constants were thus determined by nonlinear least-squares (NLLSQ) fitting using the equation:

$$RU(X) = K_A X RU_{max}/(1 + K_A X)$$

where X is the peptide concentration, RU_{max} is the maximal response unit (or equilibrium binding response), and K_A is the affinity constant. The affinity constant is defined as the ratio of the association and dissociation rate constants [$K_A = k_a/k_d$, with k_a and k_d having 1/(M s) and 1/s units, respectively].

The sensorgrams for each peptide−lipid bilayer interaction were also analyzed by curve fitting using numerical integration analysis (*37*). The BIAevaluation software offers different reaction models to perform complete kinetic analyses of the peptide sensorgrams. One curve-fitting algorithm (the two-state reaction model) was chosen on the basis of what was known about the possible binding mechanisms of lytic peptides. The data were fitted globally by simultaneously fitting the peptide sensorgrams obtained at seven different concentrations. The two-state reaction model was applied to each data set. This model describes two reaction steps (*35*) which, in terms of peptide−lipid interaction, correspond to

$$P + L \underset{k_{d1}}{\overset{k_{a1}}{\rightleftharpoons}} PL \underset{k_{d2}}{\overset{k_{a2}}{\rightleftharpoons}} PL^*$$

where, in the first step, peptide (P) binds to lipids (L) to yield PL, which is changed to PL* in the second step. PL* cannot dissociate directly to P + L and may correspond to a partial insertion of the peptide into the lipid

bilayer. The corresponding differential rate equations for this reaction model are represented by

$$dRU_1/dt = k_{a1}C_A(RU_{max} - RU_1 - RU_2) - k_{d1}RU_1 - k_{a2}RU_1 + k_{d2}RU_2$$

$$dRU_2/dt = k_{a2}RU_1 - k_{d2}RU_2$$

where RU_1 and RU_2 are the response units for the first and second steps, respectively, C_A is the peptide concentration, RU_{max} is the maximal response unit (or equilibrium binding response), and k_{a1}, k_{d1}, k_{a2}, and k_{d2} are the association and dissociation rate constants for the first and second steps, respectively, where k_{a1} has 1/(M s) units and k_{d1}, k_{a2}, and k_{d2} have 1/s units. Thus, the total affinity constant for the entire process, K, has 1/M units.

Increase in Membrane Permeability Induced by the Peptides. Membrane destabilization, which results in the collapse of the diffusion potential, was detected fluorometrically as previously described (*38*−*40*). Briefly, an LUV suspension, prepared in "K^+ buffer" (50 mM K_2SO_4/25 mM HEPES sulfate, pH 6.8), was added to an isotonic K^+-free buffer (50 mM Na_2SO_4/25 mM HEPES sulfate, pH 6.8), and the dye diS-C_3-5 was then added. The subsequent addition of valinomycin created a negative diffusion potential inside the vesicles by the selective efflux of K^+ ions, which resulted in a quenching of the dye's fluorescence ($\Delta\Psi = -142$ mV). Peptide-induced membrane permeation for all of the ions in the solution caused dissipation of the diffusion potential, manifested by an increase in fluorescence. Fluorescence was monitored using excitation and emission wavelengths at 620 and 670 nm, respectively. The percentage of fluorescence recovery, F_t, was defined by

$$F_t = [(I_t - I_o)/(I_f - I_o)] \times 100$$

where I_t = fluorescence observed after adding a peptide at time t, I_o = fluorescence after adding valinomycin, and I_f = total fluorescence before adding valinomycin.

Preparation of Bacterial Spheroplasts. E. coli spheroplasts were prepared by the osmotic shock procedure as follows: first, the cells from cultures grown to $OD_{600} = 0.8$ were harvested by centrifugation and washed twice with 10 mM Tris−H_2SO_4 and 25% sucrose, pH 7.5. Next, the cells were resuspended in the washing buffer containing 1 mM EDTA. After a 10 min incubation at 20 °C with rotary mixing, the cells were collected by centrifugation and resuspended immediately in freezing (0 °C) water. After a 10 min incubation at 4 °C with rotary mixing, the spheroplasts were collected by centrifugation and then suspended to an OD_{600} of 0.05 in a buffer containing 20 mM glucose, 5 mM HEPES, and 1 M KCl, pH 7.3.

ATR-FTIR Measurements. Spectra were obtained with a Bruker equinox 55 FTIR spectrometer equipped with a deuterated triglyceride sulfate (DTGS) detector and coupled to an ATR device as previously described (*33*). Briefly, a mixture of PE/PG (0.5 mg) alone or with peptide (∼20 μg) was deposited on a ZnSe horizontal ATR prism (80 × 7 mm). The aperture angle of 45° yielded 25 internal reflections. Prior to sample preparation, the trifluoroacetate counterions, which strongly associate with the peptides, were replaced with chloride ions through several lyophilizations of the peptides in 0.1 M HCl to eliminate an absorption band near 1673 cm^{-1} (*63*). Lipid−peptide mixtures were prepared by dissolving them together in a 1:2 MeOH/CH_2Cl_2 mixture and drying under a stream of dry nitrogen while moving a Teflon bar back and forth along the ZnSe prism. Spectra were recorded, and the respective pure phospholipid spectra were subtracted to yield the difference spectra. The background for each spectrum was a clean ZnSe prism. Hydration of the sample was achieved by introducing excess deuterium oxide (D_2O) into a chamber placed on top of the ZnSe prism in the ATR casting and incubating for 2 h before acquisition of the spectra. H/D exchange was considered complete after a total shift of the amide II band. Any contribution of D_2O vapor to the absorbance spectra near the amide I peak region was eliminated by subtracting the spectra of pure lipids equilibrated with D_2O under the same conditions.

ATR-FTIR Data Analysis. Prior to curve fitting, a straight baseline passing through the ordinates at 1700 and 1600 cm^{-1} was subtracted. To resolve overlapping bands, the spectra were processed using PEAKFIT software (Jandel Scientific, San Rafael, CA). Second-derivative spectra accompanied by 13-data-point Savitsky−Golay smoothing were calculated to identify the positions of the component bands in the spectra. These wavenumbers were used as initial parameters for curve fitting with Gaussian component peaks. Position, bandwidths, and amplitudes of the peaks were varied until (i) the resulting bands shifted by no more than 2 cm^{-1} from the initial parameters, (ii) all of the peaks had reasonable half-widths (<20−25 cm^{-1}), and (iii) good agreement between the calculated sum of all the components and the experimental spectra was achieved ($r^2 > 0.99$). The relative contents of different secondary structure elements were estimated by dividing the areas of individual peaks, assigned to a specific secondary structure, by the whole area of the resulting amide I band. The results of four independent experiments were averaged.

REFERENCES

1. Bevins, C. L., and Zasloff, M. (1990) *Annu. Rev. Biochem. 59*, 395−414.
2. Barra, D., and Simmaco, M. (1995) *Trends Biotechnol. 13*, 205−209.
3. Mor, A., Hani, K., and Nicolas, P. (1994) *J. Biol. Chem. 269*, 31635−31641.
4. Simmaco, M., Mignogna, G., and Barra, D. (1998) *Biopolymers 47*, 435−450.
5. Rinaldi, A. C. (2002) *Curr. Opin. Chem. Biol. 6*, 799−804.
6. Boman, H. G. (1995) *Annu. Rev. Immunol. 13*, 61−92.
7. Nicolas, P., and Mor, A. (1995) *Annu. Rev. Microbiol. 49*, 277−304.
8. Lehrer, R. I., and Ganz, T. (1999) *Curr. Opin. Immunol. 11*, 23−27.
9. Hoffmann, J. A., Kafatos, F. C., Janeway, C. A., and Ezekowitz, R. A. (1999) *Science 284*, 1313−1318.
10. Hancock, R. E., and Diamond, G. (2000) *Trends Microbiol. 8*, 402−410.
11. Zasloff, M. (2000) *Trends Pharmacol. Sci. 21*, 236−238.
12. Matsuzaki, K. (1999) *Biochim. Biophys. Acta 1462*, 1−10.
13. Shai, Y. (1999) *Biochim. Biophys. Acta 1462*, 55−70.
14. Bechinger, B. (1999) *Biochim. Biophys. Acta 1462*, 157−183.
15. Dathe, M., and Wieprecht, T. (1999) *Biochim. Biophys. Acta 1462*, 71−87.
16. Blondelle, S. E., Lohner, K., and Aguilar, M. (1999) *Biochim. Biophys. Acta 1462*, 89−108.
17. Epand, R. M., and Vogel, H. J. (1999) *Biochim. Biophys. Acta 1462*, 11−28.
18. Zhang, L., Scott, M. G., Yan, H., Mayer, L. D., and Hancock, R. E. (2000) *Biochemistry 39*, 14504−14514.

19. Tossi, A., Sandri, L., and Giangaspero, A. (2000) *Biopolymers 55*, 4−30.
20. Salmon, A. L., Cross, L. J., Irvine, A. E., Lappin, T. R., Dathe, M., Krause, G., Canning, P., Thim, L., Beyermann, M., Rothemund, S., Bienert, M., and Shaw, C. (2001) *J. Biol. Chem. 276*, 10145−10152.
21. Simmaco, M., Mignogna, G., Canofeni, S., Miele, R., Mangoni, M. L., and Barra, D. (1996) *Eur. J. Biochem. 242*, 788−792.
22. Simmaco, M., Mignogna, G., Barra, D., and Bossa, F. (1994) *J. Biol. Chem. 269*, 11956−11961.
23. Gazit, E., Lee, W. J., Brey, P. T., and Shai, Y. (1994) *Biochemistry 33*, 10681−10692.
24. Kliger, Y., Aharoni, A., Rapaport, D., Jones, P., Blumenthal, R., and Shai, Y. (1997) *J. Biol. Chem. 272*, 13496−13505.
25. Hultmark, D., Engstrom, A., Bennich, H., Kapur, R., and Boman, H. G. (1982) *Eur. J. Biochem. 127*, 207−217.
26. Valenti, P., Visca, P., Antonini, G., and Orsi, N. (1985) *Mycopathologia 89*, 169−175.
27. Mangoni, M. L., Miele, R., Renda, T. G., Barra, D., and Simmaco, M. (2001) *FASEB J. 15*, 1431−1432.
28. Sinclair, J. B., and Dhingra, D. (1995) *Basic Plant Pathology Methods*, 2nd ed., CRC Press, Boca Raton, FL.
29. Ohyama, T., Mugikura, S., Nishikawa, M., Igarashi, K., and Kobayashi, H. (1992) *J. Bacteriol. 174*, 2922−2928.
30. Lehrer, R. I., Barton, A., and Ganz, T. (1988) *J. Immunol. Methods 108*, 153−158.
31. Shaw, N. (1974) *Adv. Appl. Microbiol. 17*, 63−108.
32. Verkleij, A. J., Zwaal, R. F., Roelofsen, B., Comfurius, P., Kastelijn, D., and Deenen, L. V. (1973) *Biochim. Biophys. Acta 323*, 178−193.
33. Oren, Z., and Shai, Y. (2000) *Biochemistry 39*, 6103−6114.
34. Mao, D., and Wallace, B. A. (1984) *Biochemistry 23*, 2667−2673.
35. Mozsolits, H., Wirth, H. J., Werkmeister, J., and Aguilar, M. I. (2001) *Biochim. Biophys. Acta 1512*, 64−76.
36. Papo, N., and Shai, Y. (2003) *Biochemistry 42*, 458−466.
37. Morton, T. A., Myszka, D. G., and Chaiken, I. M. (1995) *Anal. Biochem. 227*, 176−185.
38. Sims, P. J., Waggoner, A. S., Wang, C. H., and Hoffmann, J. R. (1974) *Biochemistry 13*, 3315−3330.
39. Loew, L. M., Rosenberg, I., Bridge, M., and Gitler, C. (1983) *Biochemistry 22*, 837−844.
40. Shai, Y., Bach, D., and Yanovsky, A. (1990) *J. Biol. Chem. 265*, 20202−20209.
41. Wu, M., Maier, E., Benz, R., and Hancock, R. E. (1999) *Biochemistry 38*, 7235−7242.
42. Yanagida, N., Uozumi, T., and Beppu, T. (1986) *J. Bacteriol. 166*, 937−944.
43. Papo, N., Oren, Z., Pag, U., Sahl, H. G., and Shai, Y. (2002) *J. Biol. Chem. 277*, 33913−33921.
44. von Heijne, G. (1983) *Eur. J. Biochem. 133*, 17−21.
45. Trias, J., Dufresne, J., Levesque, R. C., and Nikaido, H. (1989) *Antimicrob. Agents Chemother. 33*, 1202−1206.
46. Mozsolits, H., and Aguilar, M. I. (2002) *Biopolymers 66*, 3−18.
47. Sal-Man, N., Oren, Z., and Shai, Y. (2002) *Biochemistry 41*, 11921−11930.
48. Jin, Y., Mozsolits, H., Hammer, J., Zmuda, E., Zhu, F., Zhang, Y., Aguilar, M. I., and Blazyk, J. (2003) *Biochemistry 42*, 9395−9405.
49. Mozsolits, H., Thomas, W. G., and Aguilar, M. I. (2003) *J. Pept. Sci. 9*, 77−89.
50. Byler, D. M., and Susi, H. (1986) *Biopolymers 25*, 469−487.
51. Jackson, M., and Mantsch, H. H. (1995) *Crit. Rev. Biochem. Mol. Biol. 30*, 95−120.
52. Frey, S., and Tamm, L. K. (1991) *Biophys. J. 60*, 922−930.
53. Pezolet, M., Bonenfant, S., Dousscau, F., and Papineau, Y. (1992) *FEBS Lett. 299*, 247−250.
54. Oren, Z., Hong, J., and Shai, Y. (1999) *Eur. J. Biochem. 259*, 360−369.
55. Hong, J., Oren, Z., and Shai, Y. (1999) *Biochemistry 38*, 16963−16973.
56. Sharon, M., Oren, Z., Shai, Y., and Anglister, J. (1999) *Biochemistry 38*, 15305−15316.
57. Feder, R., Dagan, A., and Mor, A. (2000) *J. Biol. Chem. 275*, 4230−4238.
58. Oren, Z., and Shai, Y. (1996) *Eur. J. Biochem. 237*, 303−310.
59. Sawyer, J. G., Martin, N. L., and Hancock, R. E. (1988) *Infect. Immun. 56*, 693−698.
60. Gazit, E., La Rocca, P., Sansom, M. S., and Shai, Y. (1998) *Proc. Natl. Acad. Sci. U.S.A. 95*, 12289−12294.
61. Shai, Y. (2002) *Biopolymers 66*, 236−248.
62. Oren, Z., and Shai, Y. (1997) *Biochemistry 36*, 1826−1835.
63. Surewicz, W. K., Mantsch, H. H., and Chapman, D. (1993) *Biochemistry 32*, 389−394.

BI034521L